INFLUENCE OF THE Al_2O_3 LAYER ON THE STRUCTURAL AND TEMPERATURE-DEPENDENT MAGNETIC PROPERTIES OF THIN COBALT FILMS

© 2025 A. V. Kobyakov[a,b,*], G. S. Patrin[a,b], V. I. Yushkov[a,b]

[a]*Siberian Federal University, Krasnoyarsk, Russia*

[b]*Federal Research Center "Krasnoyarsk Scientific Center of the Siberian Branch of the Russian Academy of Sciences", Krasnoyarsk, Russia*

**e-mail: nanonauka@mail.ru*

Received November 15, 2024

Revised December 14, 2024

Accepted December 30, 2024

Abstract. We studied cobalt films deposited by the magnetron method on an amorphous Al_2O_3 layer. The morphological and magnetic features associated with the formation of a naturally oxidized antiferromagnetic film on cobalt and the Al_2O_3/Co interface were studied. A change in the sign of the exchange bias at temperatures below 200 K was detected when the thickness of the cobalt layer on the Al_2O_3 film increased to more than 10 nm.

Keywords: *ferromagnetic film, aluminum oxide, exchange bias, interface*

DOI: 10.31857/S03676765250403e8

INTRODUCTION

In recent years, ferromagnetic metal nanoparticles have found practical applications in such fields as medicine, energy storage technologies, electronics and spintronics. Such devices are often multilayered structures with both magnetic and non-magnetic layers, with dimensions of micrometer and nanometer scales [1,2]. A large number of such devices are based on a magnetic tunnel junction consisting of two

ferromagnetic layers separated by a dielectric [3,4].

In the case of conjugation of ferromagnetic and antiferromagnetic layers, the exchange bias (EB) effect occurs when cooling below the Neel temperature. The hysteresis loop of such a structure is shifted relative to the zero external magnetic field. EB is fundamental to many practical applications. The EB effect depends on the interface features. It was proposed in [5] that atoms located near grain boundaries have fewer bonds with neighbors than atoms located in the volume. When the crystallite size decreases, the exchange interaction energy decreases and becomes comparable to the thermal energy. This leads to a disruption of the magnetic order. The behavior of magnetic moments of ferromagnetic particles becomes similar to the behavior of magnetic moments of paramagnetics. These factors, including material type and thickness, substrate type and external influences, affect the exchange coupling, the nature of the coupling mechanism between the interfaces and consequently the EB effect.

Thus, there appear problems of fundamental nature in the field of solid state physics related to the influence of structural, dimensional and interface effects, on the magnetic characteristics of thin film structures [6,7].

Earlier, in [8], the dependence of the EB effect on the thickness of wedge-shaped cobalt from 2.7 to 40 nm grown on an aluminum oxide substrate (*a-phase* $Al_{(2)}\ O_{(3)}$ $_{(}1120)$) by RF sputtering was investigated. The cobalt surface was exposed to air at room temperature. All samples had positive exchange bias below the blocking temperature and negative exchange bias near the blocking temperature. However, there is little information about the surface morphology and its relationship with the

exchange bias in the works. Therefore, the study of magnetic properties and Co/$Al_{(2)}$ $_{O3}$interface in relationship with the technological conditions of synthesis is of notable interest. In [9], the temperature dependence of magnetic properties at different sputtering rates of the structure was analyzed in the $Al_{(2)}$ $_{O(3)}$/Ge/$Al_{(2)}$ $_{O3}$/Co structure by SCVID magnetometry and the Kerr effect.

Earlier, the good applicability of the methods of magneto-optical Kerr effect and atomic force microscopy in the study of the surface and interfaces of thin layers was repeatedly shown. Thus, structural defects and spin reorientation from out-of-plane to in-plane magnetization were found in thin layers of cobalt of 8-13 monolayers in the Au/Co system [10]. In the SiO_2/Co system, the growth of cobalt film on SiO_2substrates with cobalt thickness from 1 nm and above was investigated with the formation of superparamagnetic and ferromagnetic phases [11]. In the Co/Pt system, these methods determined the contributions of interfaces and bulk materials to the magneto-optical activity [12].

In this work, we have attempted to establish by these methods the role of interfaces of a cobalt film deposited on an amorphous aluminum oxide ($Al_{(2)}$ $_{O3)}$ layer in its magnetic properties. We analyzed the behavior of the EB effect in $Al_{(2)}$ $_{O3}$-- Co bilayer structures with variable Co thickness at temperatures of 300 K and below.

EXPERIMENTAL TECHNIQUE

All investigated films were obtained by magnetron sputtering method on an ultrahigh vacuum unit of "Omicron NanoTechnology" (Germany) with turbomolecular pumps " Pfeiffer Vacuum ". The base pressure was maintained around 10^{-4}mTorr. The

working argon atmosphere had a pressure of 3 mTorr. Aluminum oxide layer was deposited by high frequency magnetron sputtering of $Al_{(2)}O_3$target (99.99%). The cobalt layer was deposited by direct current magnetron sputtering of Co target (99.95%). All targets were produced by SCOTECH LIMITED (UK).

The substrate material used was cover glass, pre-cleaned from mechanical contaminants, aged in boiling hydrogen peroxide and dried in isopropyl alcohol until complete removal of moisture. Further, to reduce roughness and irregularities, the substrate was treated by ion-plasma etching in a working chamber immediately prior to the sputtering process. To obtain more homogeneous and isotropic samples, sputtering was carried out on a rotating substrate at its temperature $T \approx 373$ K.

We obtained samples with variable Co thickness from 4 to 100 nm. The thickness of the $Al_{(2)}O_3$layer did not vary and was equal to 5 nm. In addition, to compare the samples, cobalt layers with the same thicknesses were obtained on cover glass without the $Al_{(2)}O_3$layer.The deposition rates were Co - 7.2 nm/min, $Al_{(2)}O_{(3)}$ -0.55 nm/min. The rate was controlled by the power supplied to the magnetron.

The surface morphology of the films was investigated on a VeecoMultiMode atomic force microscope. (1 nm resolution). The arithmetic mean profile deviation (R_a) and the diameter of the granules on the film surface (D) were measured. An STM-100/MF was used to control the sputtering rate and measure the thickness of the sputtered films (sputtering rate measurement resolution of 0.1 Å/s, thickness measurement resolution of - 1 Å). The results were verified by obtaining STEM images of cross sections on a Hitachi HT7700 transmission electron microscope.

Magnetic measurements were performed using the magneto-optical Kerr effect method (NanoMOKE-2). The magnetic field was directed in the film plane along the light magnetization axis. Figure 1 shows SEM images and corresponding hysteresis loops (insets) for glass/$Al_{(2)}O_3$/Co samples with cobalt layer thicknesses of 2 (a), 6 (b), 8 (c) and 10 nm (d), showing the changes with increasing cobalt thickness.

The chemical composition of the samples was studied on a SPECS electron spectrometer equipped with a hemispherical analyzer PHOIBOS 150 MCD 9 using a monochromatic Al Kα source (1486.6 eV). Spectra were processed using the CasaXPS program. The spectra were decomposed into components with a combination of Gaussian and Lorentzian lines after Shirley subtraction of the nonlinear background using the method described in [13]. As a result, a photoelectron spectrum was obtained from the surface of the cobalt film, which consists of the main components characteristic of cobalt with a fraction equal to 49.7% ($2p_{3/2}$), and oxide components with a fraction equal to 41.6%: CoO and $Co_{(3)}O_{(4)}$ (these oxides are antiferromagnetic with Neel temperatures T_N~ 290 and 40 K). These data confirm the presence of oxidized surface of the cobalt film, which is antiferromagnetic.

DISCUSSION

The dependence of the pellet diameter on the cobalt surface on the thickness of the cobalt layer (t) deposited on a layer of $Al_{(2)}O_3$, has two minima at cobalt thicknesses of about 4 and 12 nm, with a maximum at a cobalt layer thickness of about 8- 10 nm (Fig. 2a, solid line). The dependences for samples deposited on glass (dashed lines) are also presented for comparison. The dependence of the pellet diameter on the cobalt

surface on the thickness of cobalt deposited on glass has one minimum at cobalt thicknesses of about 8 nm (Fig. 2a, dashed line). As the thickness of the cobalt layer on any substrate is further increased, the pellet diameters increase up to 30-32 nm at a cobalt layer thickness of 100 nm.

Fig. 2b shows the arithmetic mean deviations of sample surface profiles (R_a) as a function of the thickness of the cobalt layer deposited on aluminum oxide deposited on glass (solid lines) and for cobalt deposited on glass (dashed line). The dependence of $R_a$in the case of the glass/$Al_{(2)}O_3$/Co sample starts from the value measured on the aluminum oxide surface R_a= 0.26 nm. In the case of the glass/Co sample, *Ra* starts from the value measured at the glass surface *Ra* = 0.32 nm. Here we note that the value of $R_a$decreased upon deposition of a 5 nm thick aluminum oxide film. This is probably due to the fact that the $Al_{(2)}O_3$coating has a higher surface energy compared to the SiO_2substrate [14]. As a result, $Al_{(2)}O_3$fills the irregularities on the substrate surface.

In general, the dependences show general patterns, but for the $Al_{(2)}O_3$/Co sample the curve is shifted towards smaller cobalt thicknesses. In both cases, *Ra* increases continuously and reaches the first maximum value at layer thicknesses of about 4 and 8 nm for Co and $Al_{(2)}O_3$/Co samples, respectively (Fig. 2). Then, the value of $R_a$decreases and reaches a minimum at a layer thickness of cobalt of about 8 and 10 nm for Co and Al_2O_3/Co samples, respectively. Then, the *Ra* value increases again and a second maximum occurs at a layer thickness of about 40-50 nm.

Since the surface free energy of cobalt is much higher than that of glass and aluminum oxide, it can be expected that the growth of cobalt follows the Vollmer-Weber mechanism. In this case, growth initially proceeds in the form of islands, with

a high rate of nucleation, followed by a period during which the rates of nucleation and growth are approximately equal. During this period, the first maximum on the cobalt thickness dependence of $R_a$is formed (at cobalt thicknesses of 4 and 8 nm for $Al_{(2)}O_3$/Co and Co samples, respectively). Thereafter, there is a slow decrease in the density of islands for thicker layers, resulting in islands merging together at higher thicknesses [15].

The second maximum on the $R_{(a)}(t)$ dependence is formed due to the following reasons. It is known that in cobalt films at thicknesses of 20-30 nm there are both non-neutral and Bloch walls. At further growth of the film up to thicknesses of about 40-60 nm, the energies of these walls coincide. At this point, the second maximum on the $R_{(a)}(t)$dependence appears. At even larger cobalt thicknesses, the energy of the Nehleff wall exceeds the Bloch wall. The shape anisotropy of these films is smaller than that of thinner films, and the perpendicular magnetocrystalline anisotropy becomes more and more significant [16].

To investigate the magnetic properties of the interfaces, magnetic hysteresis loops were measured in the temperature range from 4.2 to 300 K. The EB effect is characterized by the exchange bias field $H_{(e)}=(H_1-H_2)/2$ and the coercive force $H_{(c)}=(|H_1|+|H_{(2)}|)/2$. $H_1$and H_2correspond to the values of magnetic fields at which the magnetization of the hysteresis loop changes sign, with decreasing and increasing magnetic field strength.

Figs. 3 and 4 show the dependences of coercive forces (H_c) on temperature for the samples glass/Co (Fig. 3) and glass/$Al_{(2)}O_3$/Co (Fig. 4). For the glass/$Al_{(2)}O_3$/Co sample with a cobalt thickness of 100 nm, the hysteresis loops were measured from the

sample surface (Fig. 4 - "pov") and from the back side of the sample (Fig. 4 - "obr"). The coercive forces from the surface side and from the back side were almost the same.

Attention is drawn to the fact that for glass/$Al_{(2)}O_3$/Co samples with cobalt thickness less than 20 nm there are maxima in the $H_{(c)}(T)$dependence. As the cobalt thickness increases from 6 to 20 nm, the maximum of the dependence shifts from~ 160 to ~125 K. For cobalt layers thicker than 20 nm, no maxima are observed. For glass/Co samples, the $H_{(c)}(T)$ dependence also shows maxima at cobalt thicknesses of 10 and 20 nm at temperatures around 150 K.

Figs. 5 and 6 show the dependences of exchange displacements (H_e) on temperature for glass/Co (Fig. 5) and glass/$Al_{(2)}O_3$/Co (Fig. 6)samples. Figure 4 shows that when the thickness of cobalt on glass (glass/Co) is less than 8 nm, the magnitude of exchange bias is less than 5 E and has a positive sign in the whole temperature range (Fig. 5). But when cobalt is deposited on $Al_{(2)}O_3$layer , at the same thicknesses of cobalt, the magnitude of exchange bias has a negative sign at temperatures below ~170 K (Fig. 6). When the thickness of cobalt on the $Al_{(2)}O_3$layer is increased from 10 to 20 nm, the values of exchange displacements in both cases have positive signs and reach a maximum at temperatures around 100 K. When the thickness of the cobalt layer is further increased to 40 nm and more, the exchange displacement decreases in both cases.

For the glass/$Al_{(2)}O_3$/Co sample with a cobalt thickness of 100 nm, the exchange bias on the surface side was found to be slightly larger than that on the reverse side.

Such results, show that the exchange bias occurs due to the formation of antiferromagnetic CoO oxide layer on the cobalt surface. The contribution is significant

when the cobalt thickness is less than 20 nm of cobalt. But the variation of $H_{(e)}$ $_{(T)}$dependences for glass/$Al_{(2)\ O3}$/Co films shows that there is a contribution from the $Al_{(2)\ O3}$/Co interface as well.

It should be noted that the temperature at which the change of sign of the exchange bias occurs decreases from 190 to 160 K as the cobalt thickness increases from 6 to 10 nm in the glass/$Al_{(2)\ O3}$/Co samples.

From the analysis of the dependences of the granule diameter and $R_a$on the cobalt surface, as well as He on the cobalt thickness at room temperature, the following should be noted. The dependence of H_e, as well as the dependence of $R_a$has two maxima: in the region of 4-8 nm, as well as 40-60 nm, depending on the base on which the cobalt is deposited. The dependence of $H_e$on the pellet diameter on the cobalt surface is not observed. It is likely that the contribution of grain size to the value of exchange displacement is related not only to the change in grain size and roughness, but also to the spin structure and anisotropy of the antiferromagnet [17].

To clarify the influence of the $Al_{(2)\ O3}$/Co interface on the change of sign of the exchange bias value, additional samples were obtained. To change the surface roughness of cobalt, the cobalt deposition rate was reduced from 7.2 to 1.2 nm/min. In order to remove the influence of the CoO layer, the sputtering sequence was changed from $Al_{(2)\ O3}$/Co to Co/$Al_{(2)\ O3}$. In addition, due to the difference in melting point of Co and $Al_{(2)\ O3}$materials, a morphological change of the Co -- $Al_{(2)\ O(3)}$interface was expected.

Thus, when deposition of 10 nm thick cobalt on the $Al_{(2)\ O3}$layer at a reduced rate (from 7.2 to 1.2 nm/min), the value of the exchange displacement began to have a

negative sign only from 140 to 160 K (Fig. 6, line - 10 nm (1)). The dependence of the coercivity on temperature is presented in Figure 4 (line - 10 nm (1)).

When changing the order of deposition of glass/Co(10 nm)/$Al_{(2)\ O3}$layers, the exchange bias has a positive sign in the whole temperature range (Fig. 6, line - 10 nm (2)). In this case, the exchange shift has maximum values at a temperature of ~100 K, and the dependence of $H_{(e)\ (}T$) is similar to that for the glass/Co(10 nm) sample. It should be noted that for this thickness of cobalt, the dependence of $R_a$on the thickness of the Co layer has a maximum R_a~ 0.5 nm. The dependence of the coercivity on temperature is presented in Figure 4 (line - 10 nm (2)).

Comparison of the results of atomic force microscopy and magneto-optical measurements (analysis of $H_{(c)\ (}T$)and $H_{(e)\ (}T$) dependences) allow us to conclude about the presence of inhomogeneities both on the surface of the cobalt film and on the $Al_{(2)\ O3}$- Co interface.

For samples with reverse ordering of glass/Co/$Al_{(2)\ O3}$layers and slower Co deposition (glass/$Al_{(2)\ O3}$/Co), the $H_{(e)\ (}T$)dependence is similar to that of the Co/CoO (FM/AFM) system with a blocking temperature close to $T_{(B)\ of}$~176 K [18]. That is, these deposition regimes lead to a more planar/layered Co/$Al_{(2)\ O3}$and $Al_{(2)\ O3}$Co interface with the lowest proportion of inhomogeneities at the interface and surface.

For glass/$Al_{(2)\ O3}$/Co samples with Co thicknesses less than 10 nm deposited at an increased rate, the $H_{(e)\ (}T$) dependence is similar to that obtained from Co-CoO core-shell magnetic particles. Obviously, such a magnetic structure is formed at the $Al_{(2)\ O3}$/Co interface. The increased roughness at low Co thickness (4-5 nm) and its sharp decrease to~ 0.35 nm (at cobalt thickness ~ 8 nm), shows a sharp decrease in the

relative fraction of Co-CoO particles [19]. Thus, this deposition mode leads to the appearance of inhomogeneities both at the interface and on the cobalt surface.

Morphological inhomogeneities on the cobalt surface and in the $Al_{(2)}O_3$/Co interface lead to changes in $T_B$at Co thicknesses less than 20 nm. The increase in the share of antiferromagnetic component (oxide fraction) relative to the share of ferromagnetic component leads to an increase in T_B, approaching $T_{(N)}$(Fig. 6).

The reason for such changes in the exchange bias is most likely the porosity of $Al_{(2)}O_3$. Cobalt at 7.2 nm/min is deposited in the pores of $Al_{(2)}O_3$, forming Co-CoO core-shell particles and there is a contribution to the exchange bias from the $Al_{(2)}O_3$/Co interface. At a rate of 1.2 nm/min, the penetration depth becomes smaller and the proportion of core-shell Co-CoO particles decreases. The interface becomes similar to a layered structure. When changing the order of sputtering on Co/$Al_{(2)}O_3$, first cobalt forms a "rough" interface, and then $Al_{(2)}O_3$is deposited on it. The CoO layer is absent here. The He(T) dependence becomes positive.

CONCLUSION

The influence of the $Al_{(2)}O_3$/Co interface and the oxidized surface of the cobalt thin film deposited by magnetron method on the amorphous $Al_{(2)}O_3$layer on its magnetic properties has been investigated by atomic force microscopy, magneto-optical Kerr effect and electron spectrometry. A change in the sign of the exchange bias at temperatures below 200 K, when the thickness of the cobalt layer increases to more than 10 nm on the $Al_{(2)}O_3$film, was found. We attribute this to the formation of Co-CoO core-shell magnetic particles at the $Al_{(2)}O_3$/Co interface. When changing the order

of deposition of layers, the sign of the exchange displacement becomes positive, which is characteristic of the layered ferromagnetic/antiferromagnetic system.

The results of the work on thin film growth, under different conditions (deposition rates, rotation, substrate materials and temperatures), can provide additional information on the formation of interfaces during the growth of cobalt thin film, and can be used as recommendations for the production of multilayer structures designed for information storage, touch sensors and other devices.

FUNDING

The research was carried out within the framework of the theme of the state assignment of FGAOU VO Siberian Federal University (FSRZ-2023-0008).

REFERENCES

1. *Blauert J., Kiourti A.* // IEEE TAP. 2019. V. 68. No. 3. P. 2040.

2. *Yetisen A.K., Martinez-Hurtado J.L., Ünal B. et al.* // Adv. Mater. 2018. V. 30. Art. No. 1706910.

3. *Shkanakina M.D., Kichin G.A., Skirdkov P.N. et al. //* Bull. Russ. Acad. Sci. Phys. 2023. V. 87. No. 1. P. 92.

4. *Drovorub E.V., Prudnikov V.V., Prudnikov P.V. //* Bull. Russ. Acad. Sci. Phys. 2022. V. 86. No. 2. P. 109.

5. *Bean L.J.D.*, *Livingston C.P.* // J. Appl. Phys. 1959. V. 30. No. 4. P. 120S.

6. *Tung R.T.* // Appl. Phys. Rev. 2014. V. 1. No. 1. Art. No. 011304.

7. *Yurasov A.N., Yashin M.M., Ganshina E.A. et al. //* Bull. Russ. Acad. Sci. Phys. 2022. V. 86. No. 5. P. 601.

8. *Radu F., Etzkorn M., Siebrecht R. et al.* // Phys. Rev. B. 2003. V. 67. Art.

No. 134409.

9. *Kobyakov A.V., Turpanov I.A., Patrin G.S. et al. //* Bull. Russ. Acad. Sci. Phys. 2019. V. 83. No. 7. P. 864.

10. *Rosa R. J. G., Souza R. L., Gomes G. F. M. et al.*// AIP Advances. 2021. V. 11. Art. No. 045009.

11. *Bera A.K., Gupta P., Garai D. et al.* // Appl. Surf. Sci. Adv. 2021. V. 6. No. 1. Art. No. 100124.

12. *Demirer F.E., Lavrijsen R., Koopmans B.* // J. Appl. Phys. V. 2021. 129. Art. No. 163904.

13. *Biesinger M.C., Payne B.P., Grosvenor A.P. et al. //* Appl. Surface Sci. 2011. V. 257. P. 2717.

14. *Myers T.J., Throckmorton J.A., Borrelli R.A. //* Appl. Surface Sci. 2021. V. 569. No. 15. Art. No. 150878.

15. *Renner R. F., Liddell K., Nona C. //* J. Mater. Res. 2000. V. 15. No. 2. P. 458.

16. *Kozłowski W., Balcerski J., Kowalczyk P.J. et al. //* Appl. Phys. A. 2017. V. 123. P. 169.

17. *Nogués J., Schuller I.K. //* J. Magn. Magn. Mater. 1999. V. 192 P. 203.

18. *Gnoli L., Benini M., Del Conte C. et al. //* ACS Appl. Electron. Mater. 2024. V. 6. No. 5. P. 3138.

19. *Thomas S., Reethu K., Thanveer T. //* J. Appl. Phys. 2017. V. 122. Art. No. 063902.

FIGURE CAPTIONS

Figure 1. SEM images and corresponding hysteresis loops (insets) for glass/$Al_{(2)\,O3}$/Co samples with cobalt thicknesses of 2 (a), 6 (b), 8 (c) and 10 nm (d).

Figure 2. Dependences of the average pellet diameter (a) and arithmetic mean deviation of the profiles $R_{a)\,(b}$of the sample surfaces on the thickness of the cobalt layer at 300 K. Samples glass/$Al_{(2)\,O3}$/Co - solid line, glass/Co - discontinuous line.

Figure 3. Temperature dependences of coercive forces $H_c$for glass/Co samples, with cobalt thicknesses of 5, 7, 10, 20, 40 and 100 nm. The cobalt deposition rate is 7.2 nm/min.

Figure 4. Temperature dependences of coercive forces $H_c$for glass/ Al_2O_3/Co samples, with cobalt thicknesses of 6, 8, 10, 40 and 100 nm. The line "10 nm (1)" is for the sample with a deposition rate of 1.2 nm/min. Line "10 nm (2)" for the glass/ Co/Al_2O_3 sample . "pov" - measurements taken from the surface of the sample; "obr" - measurements taken from the back side of the sample.

Figure 5. Temperature dependences of exchange displacements $H_e$for glass/Co samples, with cobalt thicknesses of 5, 7, 10, 20, 40, and 100 nm. The cobalt deposition rate is 7.2 nm/min.

Figure 6. Temperature dependences of exchange displacements $H_e$for glass/ Al_2O_3/Co samples, with cobalt thicknesses of 6, 8, 10, 40 and 100 nm. The line "10 nm (1)" is for the sample with a deposition rate of 1.2 nm/min. Line "10 nm (2)" for the glass/Co/Al_2O_3 sample . "pov" - measurements taken from the surface of the sample; "obr" - measurements taken from the back side of the sample.

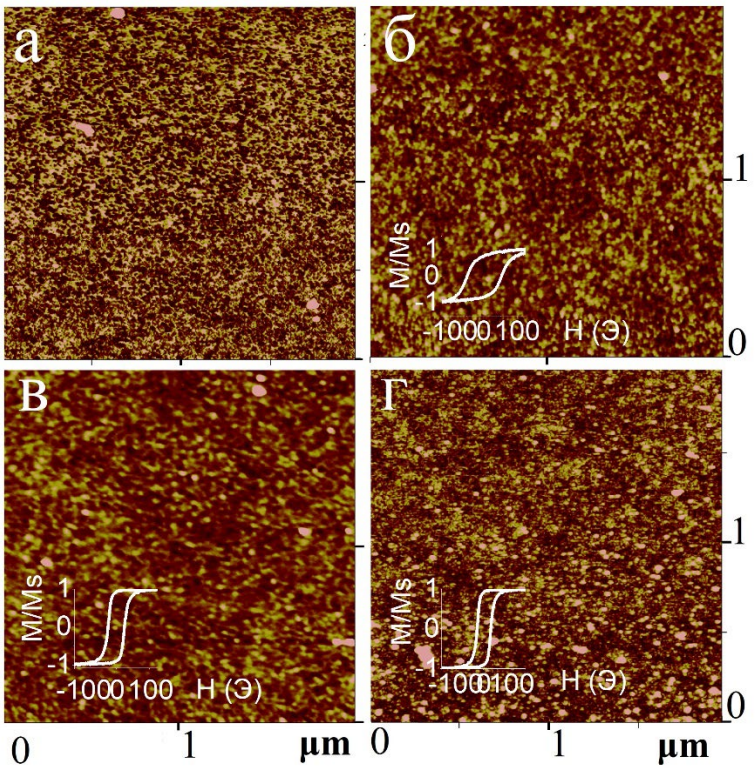
а
б
в
г
M/Ms
1
0
-1
-1000 100 H (Э)
0
1
µm

Fig. 1.

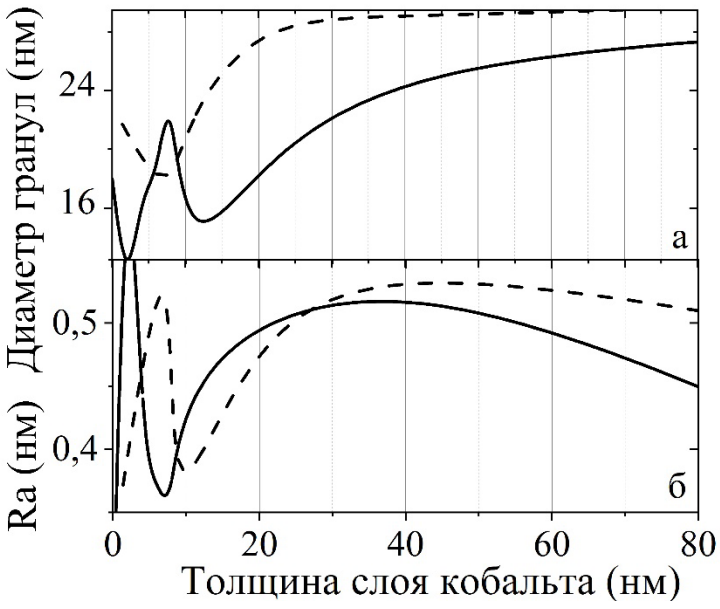
Ra (нм) Диаметр гранул (нм)
24
16
0,5
0,4
а
б
0
20
40
60
80
Толщина слоя кобальта (нм)

Fig. 2.

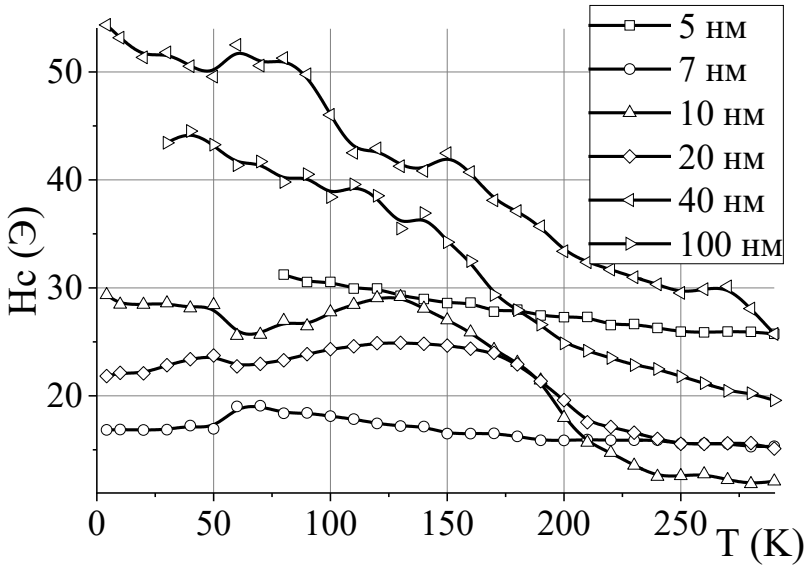
5 нм
7 нм
10 нм
20 нм
40 нм
100 нм
Hc (Э)
T (K)
50
40
30
20
0
50
100
150
200
250

Fig. 3.

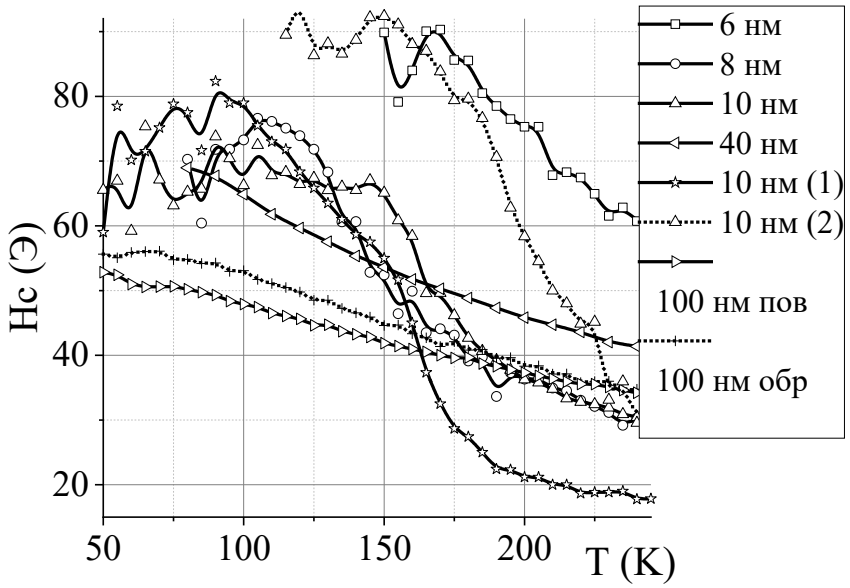
6 нм
8 нм
10 нм
40 нм
10 нм (1)
10 нм (2)
100 нм пов
100 нм обр
Hc (Э)
T (K)
80
60
40
20
50
100
150
200

Fig. 4.

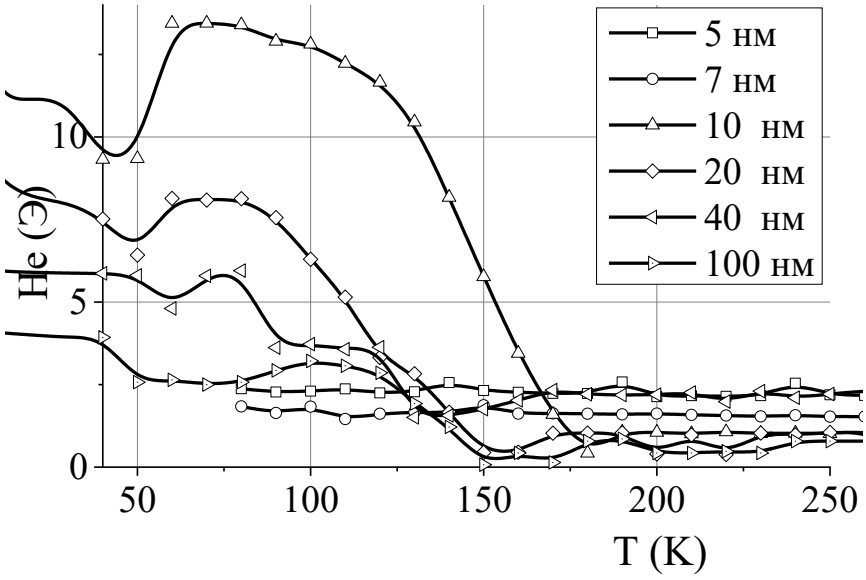
5 нм
7 нм
10 нм
20 нм
40 нм
100 нм
Hе (Э)
10
5
0
50
100
150
200
250
T (K)

Fig. 5.

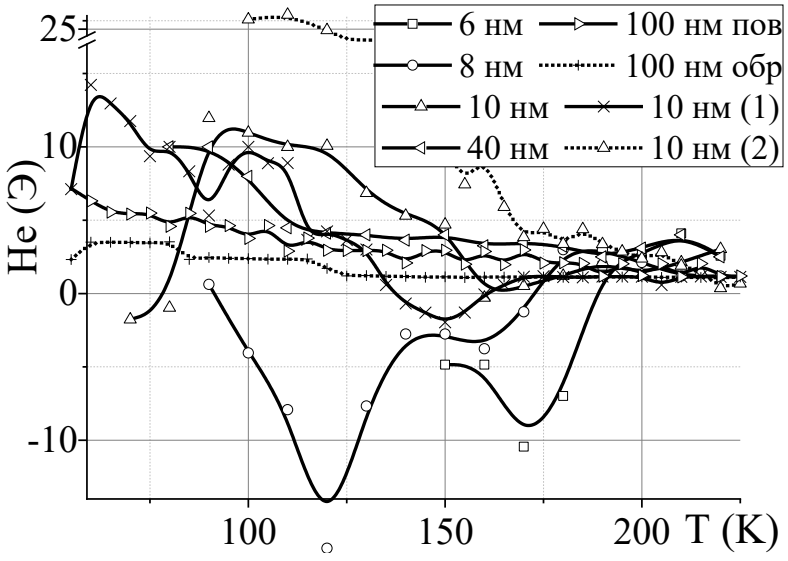
6 нм
100 нм пов
8 нм
100 нм обр
10 нм
10 нм (1)
40 нм
10 нм (2)
Hе (Э)
25
10
0
-10
100
150
200
T (K)

Fig. 6.